Allele-specific quantitative proteomics unravels molecular mechanisms modulated by *cis*-regulatory *PPARG* locus variation

Heekyoung Lee[1,2,3,4], Kun Qian[1,2,3,4,5], Christine von Toerne[4,5], Lena Hoerburger[2,6], Melina Claussnitzer[1,2,3,4,7], Christoph Hoffmann[2,8], Viktoria Glunk[1,2,3,4], Simone Wahl[4,9,10], Michaela Breier[4,9,10], Franziska Eck[5], Leili Jafari[5], Sophie Molnos[4,9,10], Harald Grallert[3,4,9,10], Ingrid Dahlman[11], Peter Arner[11], Cornelia Brunner[12], Hans Hauner[1,2,3,4,13], Stefanie M. Hauck[4,5,*] and Helmut Laumen[1,2,3,4,5,6,14,*]

[1]Else Kroener-Fresenius-Center for Nutritional Medicine, Chair of Nutritional Medicine, Technische Universität München, 85354 Freising-Weihenstephan, Germany, [2]ZIEL - Institute for Food & Health, Technische Universität München, 85354 Freising-Weihenstephan, Germany, [3]Clinical Cooperation Group Nutrigenomics and Type 2 Diabetes, Helmholtz Zentrum München and Technische Universität München, 85354 Freising-Weihenstephan, Germany, [4]German Center for Diabetes Research (DZD), Germany, [5]Research Unit Protein Science, Helmholtz Zentrum München, 85764 Neuherberg, Germany, [6]Else Kroener-Fresenius-Center for Nutritional Medicine, Paediatric Nutritional Medicine, Technische Universität München, 85354 Freising-Weihenstephan, Germany, [7]Hebrew SeniorLife Institute for Aging Research, Harvard Medical School, Boston, MA 02131, USA, [8]Else Kroener-Fresenius-Center for Nutritional Medicine, Chair of Molecular Nutritional Medicine, Technische Universität München, 85354 Freising-Weihenstephan, Germany, [9]Research Unit of Molecular Epidemiology, Helmholtz Zentrum München, 85764 Neuherberg, Germany, [10]Institute of Epidemiology II, Helmholtz Zentrum München, Neuherberg, Germany, [11]Department of Medicine, Huddinge, Karolinska Institutet, SE-141 86 Stockholm, Sweden, [12]Klinik für Hals-Nasen-Ohrenheilkunde, Universitätsklinik Ulm, 89075 Ulm, Germany, [13]Else Kroener-Fresenius-Center for Nutritional Medicine, Klinikum rechts der Isar, Technische Universität München, 81675 Munich, Germany and [14]Institute of Experimental Genetics, Helmholtz Zentrum München, 85764 Neuherberg, Germany

ABSTRACT

Genome-wide association studies identified numerous disease risk loci. Delineating molecular mechanisms influenced by *cis*-regulatory variants is essential to understand gene regulation and ultimately disease pathophysiology. Combining bioinformatics and public domain chromatin information with quantitative proteomics supports prediction of *cis*-regulatory variants and enabled identification of allele-dependent binding of both, transcription factors and coregulators at the type 2 diabetes associated *PPARG* locus. We found rs7647481A nonrisk allele binding of Yin Yang 1 (YY1), confirmed by allele-specific chromatin immunoprecipitation in primary adipocytes. Quantitative proteomics also found the coregulator RING1 and YY1 binding protein (RYBP) whose mRNA levels correlate with improved insulin sensitivity in primary adipose cells carrying the rs7647481A nonrisk allele. Our findings support a concept with diverse *cis*-regulatory variants contributing to disease pathophysiology at one locus. Proteome-wide identification of both, transcription factors and coregulators, can profoundly improve understanding of mechanisms underlying genetic associations.

INTRODUCTION

Genome-wide association studies (GWAS) identified thousands of loci associated with diverse diseases (1). The majority of variants are located in noncoding DNA regions and have been proposed to affect transcriptional regulation. Advances of the ENCODE project and novel bioinformatics approaches improved the identification of *cis*-regulatory
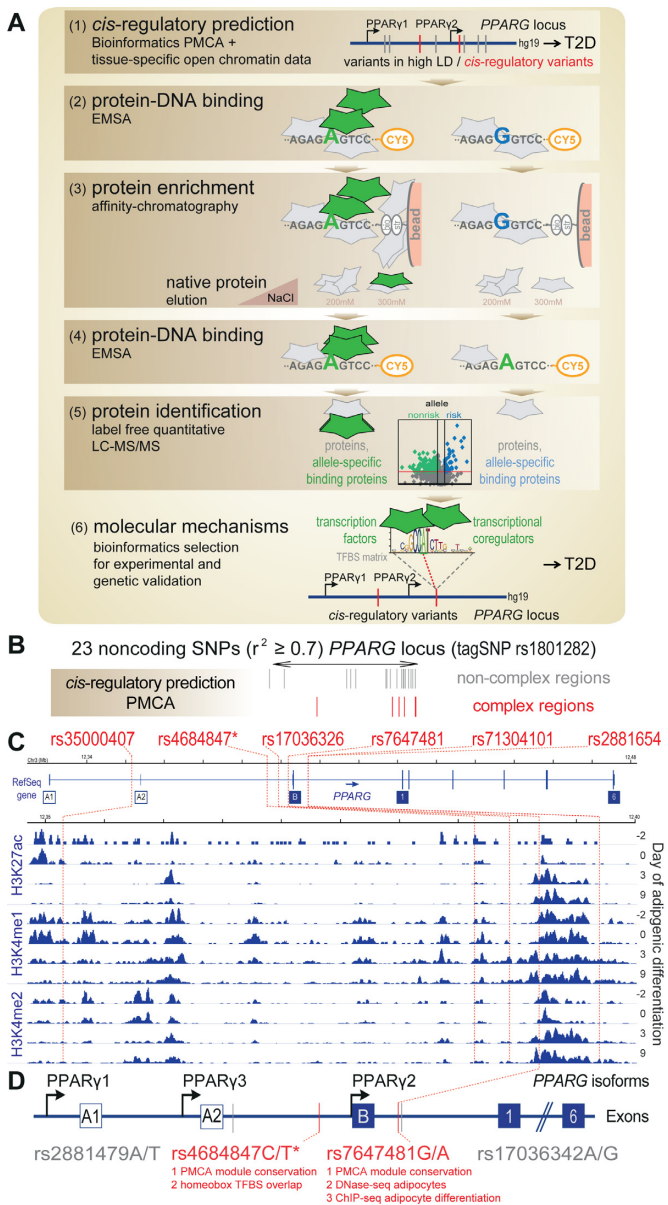

Figure 1. Discovery of allele-specific binding proteins at *cis*-regulatory variants. (**A**) Workflow: (1) *cis-regulatory variant prediction* at disease associated variants (*PPARG*) in high LD ($r^2 \geq 0.7$ (6)) by integrating bioinformatics phylogenetic TFBS module complexity analysis and regulatory chromatin marks; (2) *protein–DNA binding* assessed by Cy5 labeled oligonucleotides matching the risk and nonrisk allele, respectively, in electrophoretic mobility shift assay (EMSA); (3) *protein enrichment* with biotin (bio) labeled oligonucleotides on streptavidin-beads (str) and elution of native protein complexes with increasing concentration of NaCl; (4) *protein–DNA binding* in eluted fractions; (5) *protein identification* and quantification by LC–MS/MS and subsequent label-free quantitative analysis; and (6) molecular mechanisms, experimental and genetics verification of significant allele-specific binding transcription factors and related coregulators. (**B–D**) Bioinformatics and public domain epigenomic marks of regulatory regions infer the *cis*-regulatory variant rs7647481 at the *PPARG* locus (related to Supplementary Figure S1). (**B**) PMCA analysis of cross-species TFBS pattern conservation predicted six indicated candidate *cis*-regulatory SNPs at complex regions (6) (red) out of 23 noncoding proxy SNPs ($r^2 \geq 0.7$ (6)) at the type 2 diabetes (T2D) associated *PPARG* locus (tagSNP rs1801282). (**C**) Overlap of six variants identified in (B) with H3K27ac (histone H3-lysine 27 acetylation), H3K4me1 and H3K4me2 (histone H3–lysine 4 mono- and di-methylation) histone modification re-

variants at complex loci (2–7). Moreover, deciphering allele-specific binding of transcription factors is essential to unravel the mechanisms ultimately affecting gene expression (6,8–10). However, the identification of allele-specific binding of transcription factors and coregulators remains elusive in most cases, despite the well-established importance of a coordinated interaction between transcription factors, coregulators, and the basal transcriptional machinery for regulation of gene expression (11). Thus, in most cases the precise molecular mechanisms underlying associations between variants and disease risk remain unknown.

Quantitative protein–DNA proteomics, coupling affinity chromatography with liquid–chromatography tandem mass spectrometry (LC–MS/MS) was reported for identification of enhancer-binding proteins and for allele-specific DNA binding transcription factors (6,12,13). In this study, we introduce label-free quantitative proteomics on salt eluted sub-fractions containing native complexes, circumventing limitations of metabolic labeling strategies such as time-consuming workflows, high-costs or inefficiencies (14), or artifacts (15). The preserved allele-specific DNA-protein binding activity in the eluted sub-fractions significantly reduced complexity and allowed high coverage of quantified proteins and thereby identification of both, transcription factors and coregulators (Figure 1A).

The *Peroxisome proliferator-activated receptor gamma* (*PPARG*) locus has been robustly associated with type 2 diabetes (16–18). *PPARG* is crucial for adipogenesis, lipid metabolism, and systemic insulin sensitivity (19, 20) with the *PPARG2* isoform being mainly expressed in adipocytes (21–24). In a previous study, we reported that adipose tissue *PPARG* locus expression quantitative trait locus (eQTL) data revealed allele-specific regulation of *PPARG* expression (6). In the same study, using bioinformatics phylogenetic module complexity analysis (PMCA) we found the regulatory variant rs4684847. This variant overlaps with a homeobox transcription factor binding site (TFBS), a common feature inferred for type 2 diabetes risk variants. We further reported rs4684847C risk allele binding of the Paired Related Homeobox 1 (PRRX1) transcription factor. PRRX1 represses *PPARG* expression, and negative correlation of *PRRX1* mRNA levels with insulin-sensitivity supports contribution to insulin resistance phenotype at the *PPARG* locus (6).

In the current study, combining PMCA (6) with public domain DNase sequencing (DNase-seq) and chromatin immunoprecipitation sequencing (ChIP-seq) data we inferred rs7647481, a second *PPARG* locus *cis*-regulatory variant. We show that label-free proteomics can find both, transcrip-

---

gions at the *PPARG* locus during adipogenic differentiation of primary human adipocyte stem cells (36), GSE21366, genomic coordinates are given conform to hg19. (**D**) Localization of *cis*-regulatory (red) and non *cis*-regulatory (grey) variants subjected to workflow (A2–6) relative to transcriptional start site of the *PPARG1–3* mRNA isoforms. rs7647481 overlapping with both, day 3 and day 9, tested late stage of adipogenesis histone modification regions (Figure 1C) and with adipocyte DNase-seq regions (see Supplementary Figure S1). * rs4684847 previously identified as specifically overlapping with homeobox TFBS (6). Blue boxes = coding exons, dashed white boxes = untranslated exons, blue lines = introns, black arrows = promoters.

tion factors and cofactors at the rs7647481A nonrisk and rs4684847C risk allele, supporting the prediction of both regulatory variants. For rs7647481, we present novel experimental and human genetics data supporting the pathophysiological relevance of the transcription factor YY1 and cofactor RYBP.

MATERIALS AND METHODS

Cell culture

The SGBS human preadipocytes cell strain, primary human preadipocytes, Huh7 human hepatoma, C2C12 mouse myoblast, INS-l rat insulinoma, 293T human embryonic kidney and the HIB1B mouse brown adipocyte cell line were cultured, induced and differentiated as previously described (6,25). Ethical committee approval for primary human preadipocyte cells was obtained from the Faculty of Medicine of the Technical University of Munich, Germany.

Preparation of nuclear extracts

Nuclear protein extracts from human SGBS preadipocytes, differentiated SGBS adipocytes, and human primary preadipocytes were prepared as described (26). Briefly, cells were washed with phosphate-buffered saline (PBS), lysed in pre-chilled buffer A (10 mM HEPES pH 8.0, 10 mM KCl, 0.1 mM EDTA, 0.1 mM EGTA, 1 mM DTT, protease- and phosphatase inhibitor mix (Roche, Mannheim, Germany), 0.6% Nonidet-P40). Nuclei were collected by centrifugation, lysed in buffer B (20 mM HEPES pH 7.9, 400 mM NaCl, 1 mM EDTA, 1 mM EGTA, 1 mM DTT, 1 mM PMSF, 20% v/v glycerol, protease and phosphatase inhibitors (Roche, Mannheim, Germany), incubated on ice for 15 min, and the nuclear extract supernatant collected for further analysis. Protein concentration was quantitated using Bradford assay. HIB 1B nuclear extracts were prepared as described (25); in brief, cells were washed with PBS, lysed in pre-chilled homogenization buffer (10 mM HEPES pH 7.9, 1.5 mM $MgCl_2$, 10 mM KCl, 20 mM NaF, 0.5 mM DTT). Nuclei were collected by centrifugation, resuspended in low salt buffer (20 mM HEPES pH 7.9, 1.5 mM $MgCl_2$, 20 mM KCl, 0.2 mM EDTA, 20 mM NaF, 25% v/v glycerol, 0.5 mM DTT), lysed by adding high salt buffer containing 1.2 M KCl followed by vigorous shaking, centrifuged, and the nuclear extract supernatant was recovered for further analysis.

Oligonucleotides probes

40 bp oligonucleotides rs4684847 5′-TTTAAATCATCTC TAATTCT[C/T]ACAACTCCGAAAAGATAAG-3′; rs7647481 5′-CAACTCCCCCACTTTATTCC[A/ G]TGATGTTCAGACCCAGCCA-3′; rs17036342 5′-GCTCTCCCAAAGAATTGTAA[A/G]TTCCCAGA GTGTAGGACCA-3′; rs2881479 5′GCAAGACTCTGT CTCAAAAA[A/T]AAATAAATAAATAAATAAA-3′ with Cy5- (for EMSA) or biotin-label (for affinity chromatography) and with the respective SNP alleles at midposition were synthesized (Eurofins, Ebersberg, Germany) and annealed with unmodified complementary oligonucleotides to obtain double stranded oligonucleotides, by heating to 90°C for 5 min in TE buffer followed by slow cooling down at room temperature overnight. For competition experiments unlabeled oligonucleotides (CdxA 5′-G CATTTTATTACCACGCCTGCACTGTTGGTA-3′; MyoD 5′-CCCCCAACAGCTGTTGCCTGA-3′, Scramble 5′-AGCAAACCCTGACTAGTTATAGAGTCAAG ACCGCCCACTT-3′; YY1 5′-CGCTCCCCGGCCATC TTGGCGGCTGGT-3′) were used. Double-stranded oligonucleotides were separated from remaining single strand oligonucleotides on a 12% polyacrylamide gel.

EMSA

Non-radioactive EMSA was performed with Cy5-labeled oligonucleotide as previously described (6) with some modifications. 5 μg of nuclear protein and 0.35 μg of poly (dI-dC) (Roche, Mannheim, Germany) were used for each reaction. The reaction conditions for affinity chromatography are in general similar to those used for EMSA. To optimize DNA-protein binding in EMSAs, several conditions were tested, such as amount of proteins, concentration of the nonspecific competitor poly (dI-dC) and salt concentration in the gel binding buffer (3% (v/v) glycerol, 0.7 mM $MgCl_2$, 0.4 mM EDTA, 0.4 mM DTT, 37 mM NaCl, 0.7 mM Tris–HCl pH 7.5). In competition EMSA, 33-fold molar excess of unlabeled allele-specific probes and probes with perfect binding sites for YY1, MyoD, CdxA and a scramble oligonucleotides was added to the reaction, prior to addition of Cy5-labeled probes. Binding reactions were incubated for 20 min at 4°C. In supershift experiments, nuclear extracts were pre-incubated with 0.8 μg of anti-YY1 (sc-281x, Santa Cruz Biotechnology, Heidelberg, Germany) or isotype control IgG (sc-2027, Santa Cruz Biotechnology, Heidelberg, Germany) antibodies, respectively, for 30 min at 4°C. All EMSA experiments were replicated at least three times.

Affinity chromatography using magnetic beads

To isolate and enrich allele-specific binding proteins, we performed magnetic beads-based affinity chromatography. According to the manufacturer´s instructions, streptavidin coupled magnetic beads (Dynabeads M-280, Invitrogen, Darmstadt, Germany) were washed and collected using Bind&Wash buffer (Dynabeads M-280, Invitrogen, Darmstadt, Germany) and Magnetic particle separator (Magna-Sep™, Invitrogen, Darmstadt, Germany), discarding the supernatant. Magnetic beads were coupled to biotinylated oligonucleotides at 4°C overnight. We tested different conditions for optimal binding of beads to oligonucleotides and found that both the concentration of oligonucleotides and beads, as well as incubation time were critical for the coupling efficiency of oligonucleotides to beads. To prevent undesired reaction with streptavidin, the magnetic beads were incubated with the Bind&Wash buffer containing 8.2 μM biotin for 1 h at room temperature. The magnetic beads were then washed two times with wash buffer followed by equilibration with 1× binding buffer (10 mM Tris–HCl, 1 mM $MgCl_2$, 0.5 mM EDTA, 0.5 mM DTT, 4% v/v glycerol) and incubated with nuclear extracts for 20 min in binding buffer containing 50 mM NaCl and 0.01% CHAPS using

a rotator. We used 7 mg of nuclear extracts, which showed the most significant enrichment of proteins of interest. To reduce non-specific DNA binding, poly (dI-dC) was subsequently added to the mixture and incubated further for 10 min. Competition with poly (dI-dC) supports the specific binding of proteins to the oligonucleotides. Subsequently, the beads were washed three times with binding buffer containing 10 mM NaCl and the bound proteins were eluted by $1\times$ binding buffer with increasing concentration of NaCl (200 and 300 mM) in a volume of 100 µl (eluates E200 and E300). All steps were performed at $4°C$. Finally, 5–10 µl of protein from supernatants, washes and eluates were used for EMSA. If eluates showed enrichment of proteins of interest, the remaining volumes were subjected to LC–MS/MS analysis. All affinity chromatography experiments were replicated at least three times.

Filter-aided sample preparation (FASP) and non-targeted LC–MS/MS

Salt eluted fractions were processed as described before (10,27) in an adaptation of the FASP approach (28) using Microcon devices YM-30 (Merck Millipore, Darmstadt, Germany). The LC–MS/MS analyses were performed as described previously on a LTQ-Orbitrap XL (Thermo Scientific, Dreieich, Germany) (29) with the following adjustments: A nano trap column was used (300 µm inner diameter $\times$ 5 mm, packed with Acclaim PepMap100 C18, 5 µm, 100 Å; LC Packings) before separation by reversed phase chromatography (PepMap, 25 cm, 75 µm ID, 2 µm/100 Å pore size, LC Packings, Thermo Scientific, Dreieich, Germany) operated on a RSLC (Ultimate 3000, Thermo Scientific, Dreieich, Germany) using a nonlinear 170 min LC-gradient from 5 to 31% of buffer B (98% acetonitrile) at 300 nl/min flow rate followed by a short gradient from 31 to 95% buffer B in 5 min and an equilibration for 15 min to starting conditions. From the MS pre-scan (acquired in profile mode), the 10 most abundant peptide ions were selected for fragmentation in the linear ion trap if they exceeded an intensity of at least 200 counts and if they were at least doubly charged. Dynamic exclusion was set to 30 s. During fragment analysis, a high-resolution (60 000 full-width half maximum) MS spectrum was acquired in the Orbitrap with a mass range from 300 to 1500 Da.

Protein identification and label-free relative quantification

The RAW files (Thermo Scientific, Dreieich, Germany) were analyzed using the Progenesis LC–MS software (version 4.0, Nonlinear Dynamics, Waters, Eschborn, Germany), as described previously (29,30), with the following changes: Spectra were searched using the search engine Mascot (Matrix Science, London, UK) against the Ensembl mouse database (Release 69; 50512 sequences). False discovery rates were stringently kept below 1% as calculated by a Mascot-integrated decoy database search using the percolator algorithm (cut-off score 13, significance threshold of *P* < 0.05). Peptide assignments were re-imported into Progenesis LC–MS. Normalized abundances of all unique peptides were summed up and allocated to the respective protein.

Allele-specific YY1 Chromatin Immunoprecipitation assay (ChIP)

For each experiment, 1×10^6 primary human preadipocytes as well as preadipocytes *in vitro* differentiated to adipocytes for 14 days were cultured in six wells of a six-well plate as previously described (6). ChIP experiments were performed using the ChIP-IT® Express Enzymatic Chromatin Immunoprecipitation Kit from Active Motif (La Hulpe, Belgium) according to the manufacturer's protocol with slight modifications as described elsewhere (31). Briefly, after enzymatic digestion for 15 min, 10 mM EDTA was added and chromatin was sheared using the EpiShear™ Probe Sonicator (Active Motif, La Hulpe, Belgium; 20 pulses consisting of 20 s sonication followed by 30 s rest at 25% amplitude) in the same buffer. Chromatin was then incubated for 30 min with protein G magnetic beads (Active Motif, La Hulpe, Belgium) and 2 µg of rabbit polyclonal αYY1 antibody (sc-281x, Santa Cruz Biotechnology, Heidelberg, Germany). Incubation with 2 µg of rabbit IgG (sc-2027x) served as internal negative controls. The amount of precipitated DNA was evaluated by allele-specific quantitative PCR (AS-qPCR) using the Eppendorf Mastercycler (Eppendorf, Hamburg, Germany). To quantify allele-specific protein binding we performed SYBR-green qPCR (Maxima SYBR Green/ROX qPCR Master Mix, Thermo Scientific, Dreieich, Germany) using rs7647481 forward primer (5′-AAGATGTTTTGGGGCTTAATGG-3′) with the allele-specific reverse primers rs7647481A nonrisk (5′-G CTGGGTCTGAACATCATA̲G-3′) and G-risk (5′-CTG GGTCTGAACATCA**C**A̲G-3′), respectively (bold: SNP position, underlined: additional mutation). Allele-specific reverse primers were designed (TIB Molbiol, Berlin, Germany) with the respective rs7647481-allele and an additional mutation to increase allele-specificity as previously described (32). Allele-specificity was tested using a 611 bp DNA fragment containing rs7647481A nonrisk and G risk allele, respectively; primer efficiencies were calculated using REST 2009 software (www.gene-quantification.de/rest-2009.html). The rs7647481 allele-specific protein-chromatin interaction at the A nonrisk/G risk allele (Figure 4E) was determined by calculating $\Delta C_{t(A)}$ and $\Delta C_{t(G)}$ for A- and G-allele by subtracting the input-chromatin C_t-values from respective ChIP-chromatin C_t-values for both anti-YY1 and IgG experiments, the allele-specific ratio for each antibody based on $\Delta\Delta C_t$ method (here (primer efficiency A-allele)$^{(-\Delta C_{t(A)})}$/(primer efficiency G-allele)$^{(-\Delta C_{t(G)})}$) and finally the ratio to the respective IgG control for each experiment. Pairs of anti-YY1 and IgG ChIP experiments were performed from fixed chromatin of preadipocytes and *in vitro* differentiated adipocytes from three donors, which were previously genotyped with a concordance rate of >99.5% using the MassARRAY system with iPLEX™ chemistry (Sequenom, Hamburg, Germany) as described (33).

siRNA knock down and PCR

SGBS cells were cultured in 6-well plates and transfected with 25 nM siRNA targeting *YY1*, *RYBP* or as control non-targeting (NT) siRNA (ON-TARGETplus human siRNA SMARTpool, Dharmacon, Freiburg, Germany)

using HiPerFect (Qiagen, Hilden, Germany) according to the manufacturer's instructions. Seventy two hours after transfection, confluent cells were harvested using the RNeasy-Minikit (Qiagen, Hilden, Germany) to extract total RNA and stored at –80°C. The high capacity cDNA Reverse Transcription kit (Applied Biosystems, Darmstadt, Germany) was used for transcription of 1 μg total RNA into cDNA according to the manufacturer's instructions and stored at –20°C. RNA/cDNA concentration and purity ($A_{260/280}$) was assessed using NanoQuant Plate™ (TECAN, Männedorf, Switzerland). qPCR analysis of human *PPARG1*, *PPARG2* isoform transcripts (6), *GAPDH* housekeeping gene, *YY1* and *RYBP* to control for knockdown efficiency, was performed using the qPCR SYBR-Green ROX Mix (ABgene, Hamburg, Germany) according to the manufacturer's instructions, using a Mastercycler Realplex 4 and Realplex Software (Eppendorf, Hamburg, Germany) with an initial activation of 15 min at 95°C followed by 40 cycles of 15 s at 95°C, 30 s at 60°C and 30 s at 72°C. Amplification of specific transcripts was confirmed by initial sequencing, and melting curve profiles (cooling samples to 68°C and heating slowly to 95°C with measurement of fluorescence) and by agarose gel electrophoresis to assess the size of PCR products. *PPARG1* (NM_138712.3): forw5′-CGTGGCCGCAGATTTGA-3′ + rev5′-AGTGGGAGTGGTCTTCCATTAC-3′ = 177bp; *PPARG2* (NM_015869.4): forw5′-GAAAGCGAT TCCTTCACTGAT-3′ + rev5′-TCAAAGGAGTGGG AGTGGTC-3′ = 146bp; *GAPDH* (NM_002046.5): forw5′-GATCATCAGCAATGCCTCCTGC-3′ + rev5′-ACAGTCTTCTGGGTGGCAGTGA-3′ = 128bp; *RYBP* (NM_012234.6): forw5′-CTGCACCTT CAGAAACAGTGC-3′ + rev5′-GTGCCACCAGC TGAGAATTG-3′ = 103 bp; *YY1* (NM_003403.4): forw5′-CGAGTTCTCGGTCACCATGT-3′ + rev5′-CTGCCAGTTGTTTGGGATCT-3′ = 181 bp (specificity of primer tested by BLAST). Mean target mRNA levels, standardized to gene expression levels of the housekeeping gene, from five independent biological replicates of knockdown experiments, each PCR measured in duplicates, were calculated using the $\Delta\Delta C_t$ method relative to the siNT control experiment. *P*-values were calculated using one-sample *t*-test.

Luciferase reporter gene assays

To assess transcriptional activity mediated by SNP-adjacent regions, luciferase reporter gene assay was performed as described previously (6) with the following modifications. C2C12 cells cultured in 48-well plates to approximately 80% confluence were differentiated for 7 days as described above. C2C12 cells (undifferentiated myoblasts, differentiated myocytes), 293T, INS-1 β and Huh7 cells at 80–90% confluence were transfected in 48-well plates by Lipofectamine 2000 transfection reagent (Invitrogen, Darmstadt, Germany). 293T, Huh7, and C2C12 (undifferentiated and differentiated) were transfected with 0.3 μg of the respective firefly luciferase reporter vector, 0.04 μg of the ubiquitin promoter vector and 1 μl of Lipofectamine 2000 reagent. INS-1 β-cells were transfected with 1.2 μg of the respective firefly luciferase reporter vector, 0.16 μg of the

ubiquitin promoter vector and 2 μl of Lipofectamine 2000 reagent. 3–4 h after transfection the medium was replaced by fresh medium followed by incubation at 37°C. Twenty four hours after transfection, the cells were washed once with PBS and lysed in 1× passive lysis buffer (Promega, Mannheim, Germany) on rocking for 20 min at room temperature. Firefly and renilla luciferase activity were measured using luminometer (Berthold, Pforzheim, Deutschland), respectively. The ratios of firefly luciferase expression to renilla luciferase expression were calculated and normalized to the thymidine kinase promoter control vector. All experiments were performed repeatedly as indicated. *P*-values were calculated using paired *t*-test.

GO-term, signaling pathway and transcription factor/transcriptional coregulator co-citation analysis

The Genomatix GePS-tool (Genomatix, Munich, Germany) was used to assess the enrichment of molecular function GO-terms (Supplementary Table S2) and signaling pathways (Supplementary Table S3) in the protein/gene data sets identified by LC–MS/MS, using all identified proteins. Next, to calculate the enrichment of transcriptional coregulators, we used the Genomatix GePS-tool to build a co-citation based network. All proteins annotated as cofactors (Supplementary Table S4) and the respective candidate transcription factors *PRRX1*, *YY1* and *NFATC4* were used as input gene list to create networks using the settings co-citation level: *Function word level*; co-citation filter: (i) Network generation: *simple network*; and additional interactions per gene: (ii) Genes with interactions are shown in the Figure 5A and Supplementary Figure S5A-C.

Regression analysis of human adipose tissue samples

The insulin-resistance measure HOMA-IR (homeostasis model assessment of insulin resistance) and mRNA expression levels were measured in a cohort comprising 30 obese (BMI > 30 kg/m^2) otherwise healthy and 26 non-obese (BMI < 30 kg/m^2) healthy women (34), all premenopausal and free of continuous medication and investigated in the morning after an overnight fast. Venous blood sample was obtained for measurements of glucose, insulin and for preparation of DNA. HOMA-IR was calculated by the formula fP-Glucose (mmol/L) × (fS-Insulin (microU/ml)/ 22.5) (35). Following blood sampling abdominal subcutaneous adipose tissue biopsy was obtained by needle aspiration and adipose microarray analysis was performed exactly as described (34) using the Affymetrix GeneChip Array protocol with 1 μg of total adipose RNA from each subject (gene expression deposited in the National Center for Biotechnology Information Gene Expression Omnibus (GEO; https://ncbi.nlm.nih.gov/geo/) and accessible using GEO series accession number GSE25402). Linear regression analyses were performed with R, version 3.0.2 (R: A Language and Environment for Statistical Computing: from the R Development Core Team of the R Foundation for Statistical Computing, Vienna, Austria, 2014, http://www.R-project.org/) to assess correlation of *YY1*, *RYBP* and *PPARG* adipose tissue mRNA levels with HOMA-IR (adjusted for age, age/BMI and without
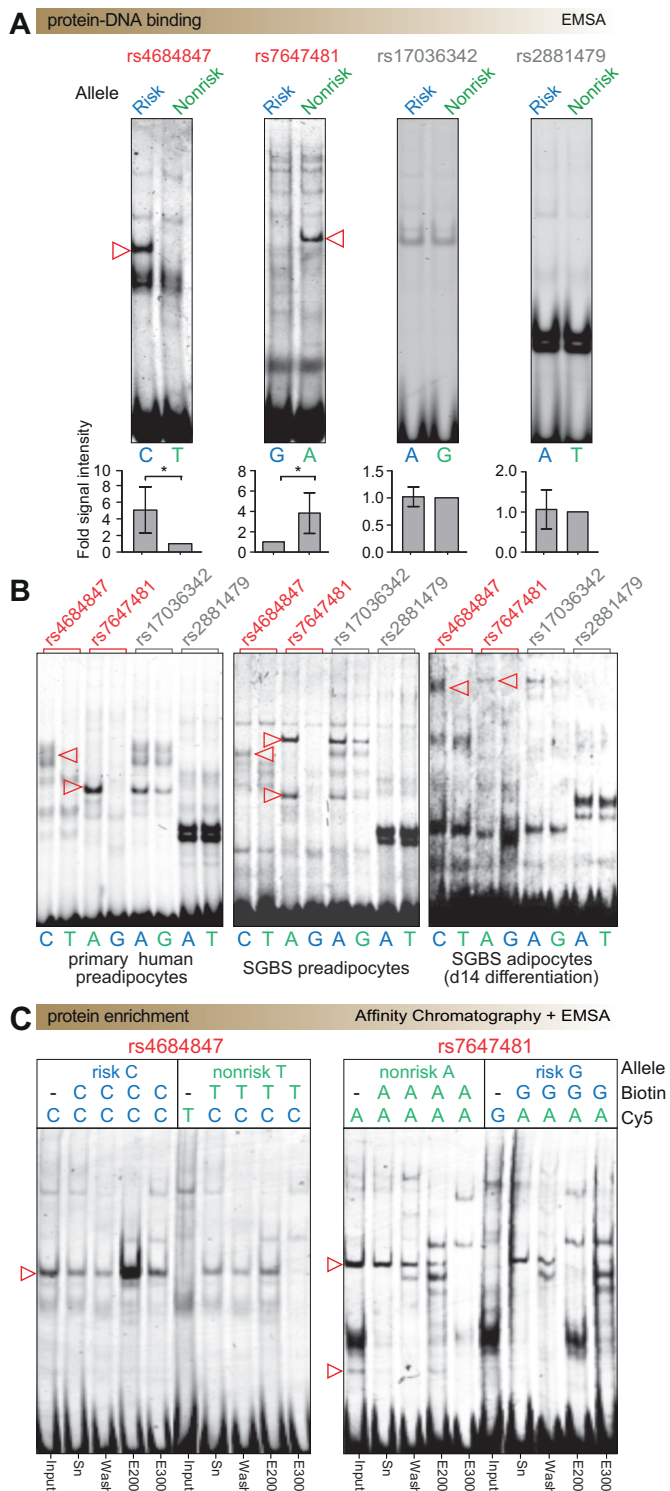
Figure 2. Enrichment of risk and nonrisk allele-specific binding proteins at predicted *cis*-regulatory SNPs. (**A**) Representative EMSA experiments with allele-specific Cy5-labeled probes on nuclear extracts from HIB 1B cells (triangle = allele-specific band) demonstrated allele-specific differential binding affinity of proteins at the risk/nonrisk allele of predicted *cis*-regulatory rs4684847/rs7647481 variants (red), respectively, and no binding at predicted non *cis*-regulatory SNPs (grey). Bar charts illustrate the allelic fold change of protein–DNA complexes signal intensity (allele with highest binding/allele with lowest binding; allele with lowest binding set to one), mean ± SD of five experiments. *$P < 0.05$. *P*-value by paired

adjustment) for 20 risk allele and 18 nonrisk allele carriers with available genotypes. Adipose tissue samples were genotyped for rs1801282, rs4684847 and rs7647481 with a concordance rate of >99.5% using the MassARRAY system with iPLEX™ chemistry (Sequenom, Hamburg, Germany), as previously described (6,33). The study was approved by the local ethics committee of the Karolinska University Hospital, Stockholm, Sweden; written informed consent was obtained from all patients who donated biological samples.

Statistical analysis

All results were expressed as mean ± SD. Student´s *t*-tests, Wilcoxon signed rank test and one-sample *t*-tests were used to compare two groups (two alleles/complex and non-complex SNP regions). All statistical analyses were performed using the Graph Pad Prism software v5.02 (Graph-Pad Software, CA, USA) or the Statistical Software SPSS v20.0 (IBM Corporation, NY, USA). The applied statistical methods for each experiment are given in the respective figure legend. Statistical differences of results were shown in *$P < 0.05$, **$P < 0.01$, ***$P < 0.001$.

RESULTS

Risk and nonrisk allele-specific protein–DNA interaction at the *cis*-regulatory variants rs4684847 and rs7647481

At the *PPARG* locus, with a total of 23 non-coding variants in high linkage disequibrilium ($r^2 \geq 0.7$ with *PPARG* tagSNP rs1801282 (6)), six variants were predicted to be *cis*-regulatory by conserved binding site modularity analysis (Figure 1B). We showed previously that rs4684847 specifically overlaps with a homeobox TFBS and modulates regulation of *PPARG* expression (6). Further assessing proximity of the remaining five variants to marks of regulatory regions in adipocytes, we find rs7647481 to overlap with all histone modification regions (36) at both tested late stages (day 3 and day 9) of human adipogenesis (Figure 1C), and with DNase-seq regions (2) in differentiated primary human adipocytes (Supplementary Figure S1); supporting a contribution of rs7647481 to adipocyte specific *PPARG2*

t-test. (**B**) Risk and nonrisk allele protein–DNA interaction at predicted *cis*-regulatory and non *cis*-regulatory SNPs in human preadipocytes and adipocytes. EMSA with allelic Cy5-labeled probes for the indicated predicted *cis*-regulatory (red) and non *cis*-regulatory (grey) SNPs using nuclear extracts from undifferentiated primary human preadipocytes (left panel), the human SGBS preadipocyte cell line (mid panel) and SGBS cells *in vitro* differentiated to adipocytes for 14 days (right panel). (**C**) Enrichment of allele-specific differential binding proteins. EMSA with binding-allele specific Cy5-labeled probes of predicted *cis*-regulatory SNPs using protein from affinity chromatography with the respective biotin-labeled risk/nonrisk allelic-probes. Triangle = allele-specific band; input: nuclear protein used for affinity chromatography; Sn: supernatant after incubation with biotin-labeled allelic-probe-magnetic beads conjugates; Wash: low NaCl concentration wash eluates; E200/E300: 200 and 300 mM NaCl protein eluates used for LC–MS/MS. Protein eluates E200 and E300 with differential protein–DNA binding contain the prioritized transcription factors YY1 at rs7647481A nonrisk and PRRX1 at rs4684847C risk allele (Table 1). All experiments were performed in triplicates. For enrichments at predicted non *cis*-regulatory SNPs, see Supplementary Figure S2.

expression (Figure 1D). Both, rs7647481 and the previously reported rs4684847 (6) are in perfect linkage disequilibrium ($r^2 = 1.0$ in 1000 Genomes (37)), confirmed by sequencing in this study for all analysed tissues and cells (data not shown). To experimentally evaluate these *cis*-regulatory predictions, we further analysed allele-specific protein–DNA interactions at both predicted *cis*-regulatory variants and additionally at two variants predicted as non *cis*-regulatory (Figure 1D).

Electrophoretic mobility shift assays (EMSA) using nuclear extracts of mouse brown adipocytes, revealed allele-specific protein–DNA interaction for both predicted *cis*-regulatory SNPs, not observed with the predicted non *cis*-regulatory SNPs (Figure 2A upper panel). Quantification of protein–DNA complexes confirmed allele-specific binding at both predicted *cis*-regulatory SNPs ($P = 0.03$) in contrast to non *cis*-regulatory SNPs ($P = 0.82$ for rs17036342 and $P = 0.80$ for rs2881479, respectively) (Figure 2A lower panel). *PPARG* regulates adipogenesis and mature adipocyte metabolism. In EMSA experiments using nuclear protein extract from primary human preadipocytes, human SGBS cell strain preadipocytes and *in vitro* differentiated SGBS adipocytes, we find differential protein–DNA interaction patterns (Figure 2B), indicative for different transcription factors and regulatory protein complexes contributing to *PPARG* expression in different stages of adipogenesis. Allele-specific differential binding was observed consistently at predicted *cis*-regulatory variants, with increased binding at rs7647481A nonrisk and rs4684847C risk allele, respectively.

Identification of allele-specific binding proteins at predicted *cis*-regulatory variants by label-free quantitative proteomics

Next, we aimed to identify allele-specific binding proteins, i.e. regulators and coregulators at those variants by an unbiased, quantitative label-free protein–DNA proteomics (Figure 1A-5). To enrich allele-specific binding proteins for identification by mass spectrometry, we incubated biotinylated oligonucleotides of 40 bp length with risk or non-risk allele of each SNP at midposition with nuclear extracts. DNA-binding proteins were concentrated by affinity chromatography with streptavidin coupled to magnetic beads. We performed a fractionation approach using increasing elution stringency of the native protein complexes, enabling direct control for an enrichment of allele-specific binding proteins in the eluted fractions by EMSA assays prior to LC–MS/MS analysis. This mass spectrometric analysis of the relevant fractions effectively reduced complexity, and thus enabled specific detection of both, transcription factors and transcriptional coregulators (Figure 1A-6, see also chapter on YY1 transcription factor and RYBP cofactor at rs7647481). EMSA experiments with bead-eluted proteins revealed an enrichment of allele-dependent protein DNA-binding complexes for both predicted *cis*-regulatory SNPs, by increased binding to the rs4684847C risk and to the rs7647481A nonrisk allele (Figure 2C). Protein eluates from predicted non *cis*-regulatory SNPs revealed no obvious allelic differences (Supplementary Figure S2).

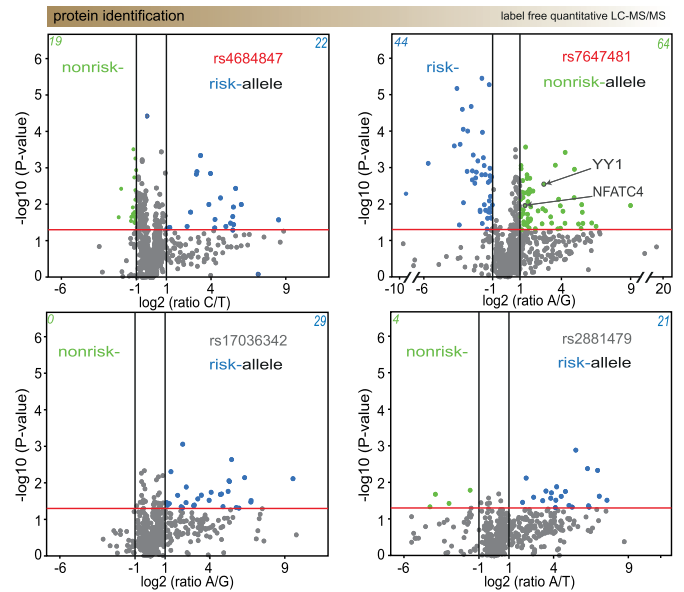At predicted *cis*-regulatory SNPs, LC–MS/MS found 41–108 and 142–165 proteins (Figures 3 and Supplemen-

Figure 3. Label-free quantitative LC–MS/MS proteomics identified risk versus nonrisk allele-specific binding proteins at predicted *cis*-regulatory and non *cis*-regulatory SNPs. Volcano plots for the indicated variants illustrate the distribution of risk (blue) and nonrisk (green) allele-specific binding proteins identified by LC–MS/MS (results from 200 mM NaCl eluates illustrated by EMSA in Figure 2C and Supplementary Figure S2, results from 300 mM eluates see Supplementary Figure S3) at predicted *cis*-regulatory (red) and non *cis*-regulatory SNPs (grey). Proteins with significant ($P \le 0.05$, red line) allele-specific differential binding (allelic ratio ≤ 0.5 or ≥ 2) at the risk allele = blue dots, nonrisk allele = green dots; with no significant allele-specific binding = grey dots; n of proteins per quadrant = *italic* numbers. Arrows highlight proteins from Table 1 annotated as transcription factors with fold change ≥ 2, $P \le 0.01$, number of identified peptides ≥ 2. Mean protein levels ($\log_2$ ratio of indicated alleles) and P-value from unpaired t-test of three independent experiments.

tary Figure S3, respectively, upper panels) with a significant allele-specific binding (fold change ≥ 2, $P \le 0.05$, $n = 3$, t-test), in contrast to 25–29 and 44–82 proteins at predicted non *cis*-regulatory SNPs (lower panels). Comparing the numbers of allele-specific binding proteins at predicted *cis*- versus non *cis*-regulatory variants, we found a significant enrichment of differentially binding proteins at *cis*-regulatory variants ($1.87 \times 10^{-25} \le P \le 1.72 \times 10^{-6}$, two-sided, two-group binomial test for pairwise comparison of differentially binding proteins, Supplementary Table S1). The comparison of predicted *cis*- versus *cis*-regulatory and non *cis*- versus non *cis*-regulatory SNPs revealed no significant enrichment for most pairs ($4.26 \times 10^{-4} \le P \le 0.28$, Supplementary Table S1). Thus, the highest numbers of allele-specific binding proteins were found at predicted *cis*-regulatory SNPs supporting specific protein–DNA interaction (Figure 2A). Moreover, when assessing GO-terms for allele-specific binding proteins (fold change ≥ 2, $P \le 0.05$), we found a significant enrichment in the GO-terms *DNA binding proteins* ($P = 1.36 \times 10^{-6}$, $P = 1.44 \times 10^{-7}$) and *structure-specific DNA binding proteins* ($P = 2.11 \times 10^{-5}$, $P = 3.69 \times 10^{-8}$) at the predicted *cis*-regulatory variants rs4684847 and rs7647481 in contrast to low respective GO-term enrichment at predicted non *cis*-regulatory vari-

Table 1. Allele-specific differentially binding transcription factors

SNP	Gene symbol	Allelic ratio	Allelic fold change	P-value (fold change)	Quantified peptides
rs7647481	YY1	A/G	6.6	2.94×10^{-3}	9
	NFATC4		2.6	0.01	2
rs4684847	PRRX1	C/T	2.6	0.01	5
	ILF3		4.2	0.01	4

Proteins annotated as transcription factors and identified by LC–MS/MS in the fractions with the highest allelic protein–DNA binding EMSA signal intensity after affinity-chromatography enrichment at rs7647481A nonrisk and rs4684847C risk allele (Figures 2C, 200 and 300 mM elution, respectively) and significant differential binding (allelic fold change ≥ 2.0, P-value ≤ 0.01, illustrated in Figure 3 and Supplementary Figure S3) are shown.

ants ($4.44 \times 10^{-3} \leq P \leq 0.04$, and $1.47 \times 10^{-3} \leq P \leq 9.43 \times 10^{-3}$, Fisher´s exact test, Supplementary Table S2).

Focusing on transcription factors identified at the novel *cis*-regulatory variant rs7647481, label-free proteomics found the nonrisk allele binding transcription factors YY1 with a 6.6-fold ($P = 2.94 \times 10^{-3}$) and NFATC4 with a 2.6-fold ($P = 0.01$) allelic fold-change (Table 1, Figure 3). For rs4684847, previously shown to abrogate a type 2 diabetes-specific homeobox TFBS and to infer with PRRX1 homeobox protein binding (6), proteomics found increased risk allele binding of PRRX1 and ILF3 (2.6-fold, $P = 0.01$ and 4.2-fold, $P = 0.01$, respectively, Table 1, Supplementary Figure S3). Subsequently, we assessed the enrichment of canonical signaling pathways using the GePS-tool (Genomatix) within the set of all identified allele-specific binding proteins and the occurrence of candidate transcription factors in the identified pathways (Supplementary Table S3). Notably, the only transcription factor identified in our screen included in significantly enriched signaling pathways was YY1 ($P < 0.05$, Fisher´s exact test, *E2f transcription factor network*, *p53 pathway*, *Prc2 complex sets long-term gene silencing through modification of histone tails*, and *signaling events mediated by HDAC Class I*).

YY1 drives transcriptional activity at the rs7647481A nonrisk allele of the *PPARG* locus

The common rs7647481G risk allele abrogates the core of a YY1 consensus TFBS, confirming the mass spectrometric identifications and GO-term analyses (Figure 4A). The allele-specific protein–DNA interaction at the rs7647481-adjacent region was efficiently blocked in competition and supershift EMSA experiments by 33-fold molar excess of unlabeled YY1 consensus binding sequence or by pre-incubation with a YY1 specific antibody (Figure 4B left panel), while protein binding was not affected at all other tested SNP-adjacent regions, including the *cis*-regulatory variant rs4684847 (Figure 4B). Competition with unspecific competitor oligonucleotides (consensus *MyoD* myogenic regulatory factors, consensus *CdxA* chicken homeodomain protein, and scrambled control sequence) did not affect the allele-specific protein binding (Supplementary Figure S4A), further confirming the specificity of YY1 binding at the rs7647481-adjacent region. *PPARG* expression is essential for preadipocyte differentiation and metabolic function of mature adipocytes. By YY1 competition and supershift experiments we confirmed YY1 binding at the rs7647481A nonrisk allele in both, 3T3-L1 preadipocytes and adipocytes (Supplementary Figure S4B). In reporter gene assays with luciferase constructs of all tested variants transfected into 293T cells, overexpression of the transcrip-

tion factor YY1 revealed a significant higher transcriptional activity at the rs7647481A nonrisk allele as compared to the risk allele ($P = 0.003$, Figure 4C). Although we found an overall increase of all tested reporters, no allele-specific effects of the *cis*-regulatory variant rs4684847 and both non *cis*-regulatory variants were observed. The rs7647481A nonrisk variant also increased transcriptional activity in different cell types significantly, i.e. by 1.2-fold in 293T cells, 1.4-fold in INS1 β-cells, 2.7-fold in C2C12 myoblasts, 2.2-fold in C2C12 myocytes, 1.3-fold in Huh7 hepatocytes ($P < 0.01$, Figure 4D) and 1.5-fold in 3T3-L1 adipocytes (6).

Next, we aimed to confirm *in vivo* allele-specific binding of YY1 at the rs7647481A nonrisk allele, as results from reporter assays are limited by missing chromosome context or length of analysed sequences. We performed chromatin immunoprecipitation (ChIP) combined with allele-specific quantitative PCR (AS-qPCR) to test for allelic imbalance in primary human adipose tissue cells heterozygous for rs7647481G/A. ChIP experiments were performed using a YY1-specific antibody to pull down cross-linked YY1-protein / chromatin complexes from primary human preadipocyte and adipocyte cells of three donors (Figure 4E). In both, input chromatin and immuno-precipitated chromatin, the nonrisk and risk allele, respectively, were analyzed using AS-qPCR. In adipocytes we observed a significant mean 31.8-fold ($P = 0.02$, Wilcoxon signed rank test) increased binding of YY1 at the rs7647481A nonrisk allele as compared to the risk allele in chromatin immuno-precipitated with anti-YY1. In preadipocytes, we observed a large variation of YY1 binding at the nonrisk allele but no significant allele-specific binding. No allele-specific differences were observed when using an IgG control antibody. Overall, YY1 supershift (Figure 4B, Supplementary Figure S4B) and ChIP (Figure 4E) experiments in preadipocytes and adipocytes establish binding of the transcription factor YY1 at the rs7647481A nonrisk allele, and support its role in transcriptional regulation of the *PPARG* gene in both stages of adipogenesis.

Identification of transcription factor related transcriptional coregulators

Metabolic homeostasis is largely regulated at the transcriptional level through the coordinated interaction between transcription factors, coregulators, and the basal transcriptional machinery (11). Our pull down of protein–DNA binding complexes offers the opportunity to identify functional protein–DNA interactions as we found both, transcription factors (Table 1) and co-eluting transcriptional coregulators (Supplementary Table S4). We assessed relevant protein-protein interaction using literature co-citation
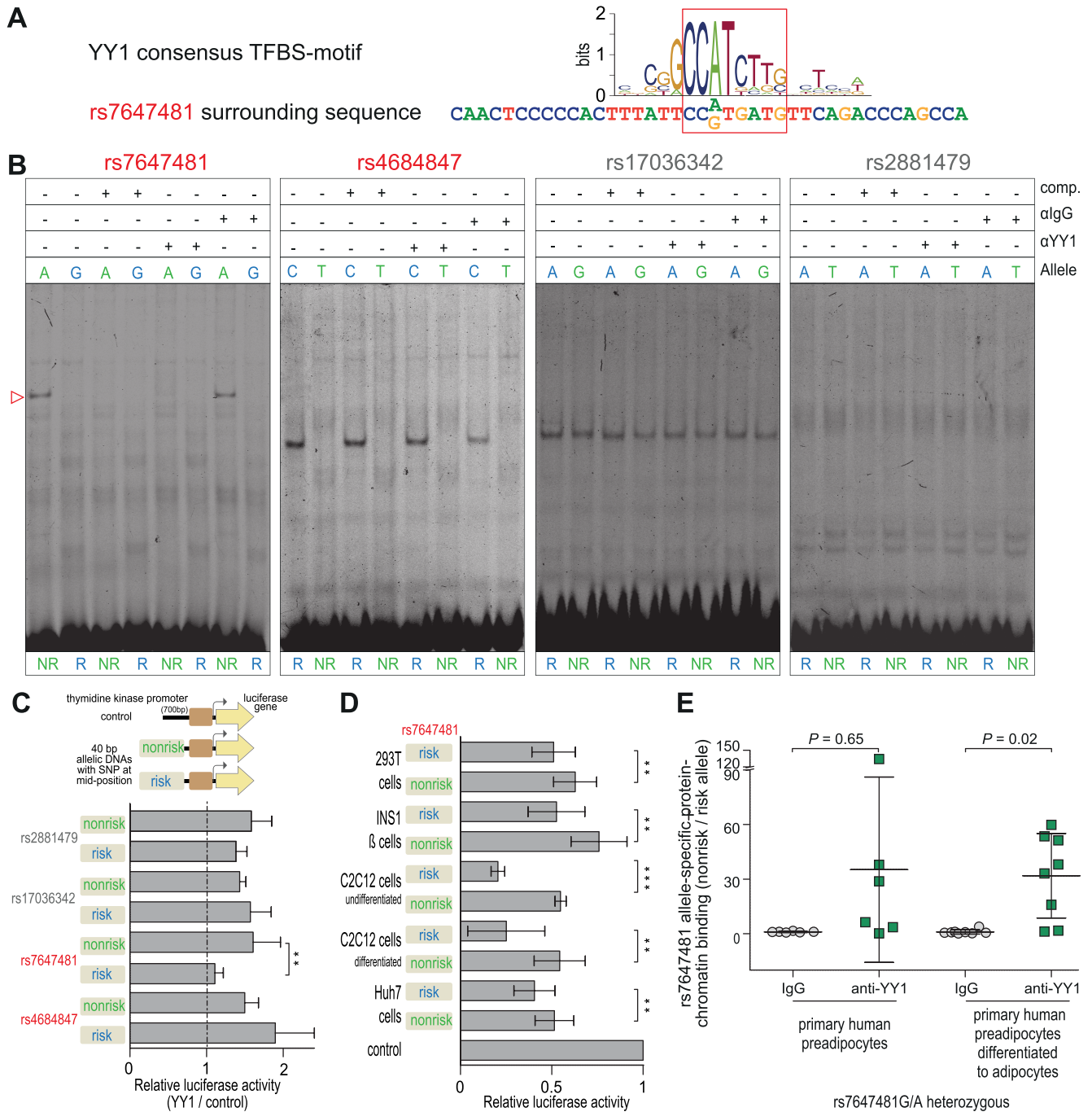
Figure 4. rs7647481A nonrisk allele-specific binding and transcriptional activity of the transcription factor YY1 inferred from proteomics analysis. (**A**) The rs7647481G risk allele abrogates the core of a YY1 consensus binding site (Matbase Matrix Library 9.1, Genomatix. Munich, Germany). (**B**) Competition and supershift EMSA experiments using risk (**R**) and nonrisk (**NR**) allele-specific Cy5-labeled probes of the predicted *cis*-regulatory (red) and non *cis*-regulatory (grey) variants reveal a specific binding of YY1 at the rs7647481A nonrisk allele. Competition (comp.) assays using 33-fold excess of unlabeled YY1 probe and supershift assays by adding anti-YY1 (αYY1) or IgG isotype control antibody, respectively. (**C**) Reporter assays in 293T cells with constructs harbouring the risk and nonrisk allele of predicted *cis*-regulatory (red) and non *cis*-regulatory (grey) variants reveal allele-specific activation from the rs7647481A nonrisk allele upon YY1 overexpression. Mean ± SD from five experiments. (**D**) rs7647481A nonrisk allele-specific activation of reporter gene activity in 293T-cells, INS-1 β-cells, C2C12 cells (undifferentiated myoblasts, differentiated myocytes) and Huh7 hepatocytes assessing the effect of endogenous transcriptional regulators. Reporter assays with luciferase constructs containing the respective allele at midposition as indicated; for each cell line the TK-promoter control vector was co-transfected separately and set to one. Mean ± SD from seven experiments. (**E**) Increased *in vivo* YY1 binding at the rs7647481A nonrisk allele. The result shows allele-specific binding at the A-nonrisk/G-risk allele, determined by ChIP experiments in primary human adipose tissue cells, preadipocytes and *in vitro* differentiated adipocytes, heterozygous for rs7647481G/A using αYY1 or IgG isotype control, respectively, followed by allele-specific qPCR detecting the rs7647481A nonrisk and G risk allele for each ChIP experiment (see also Materials and Methods). Mean ± SD from ChIP experiments using chromatin–DNA from three donors, *P*-values from Wilcoxon's signed rank test.
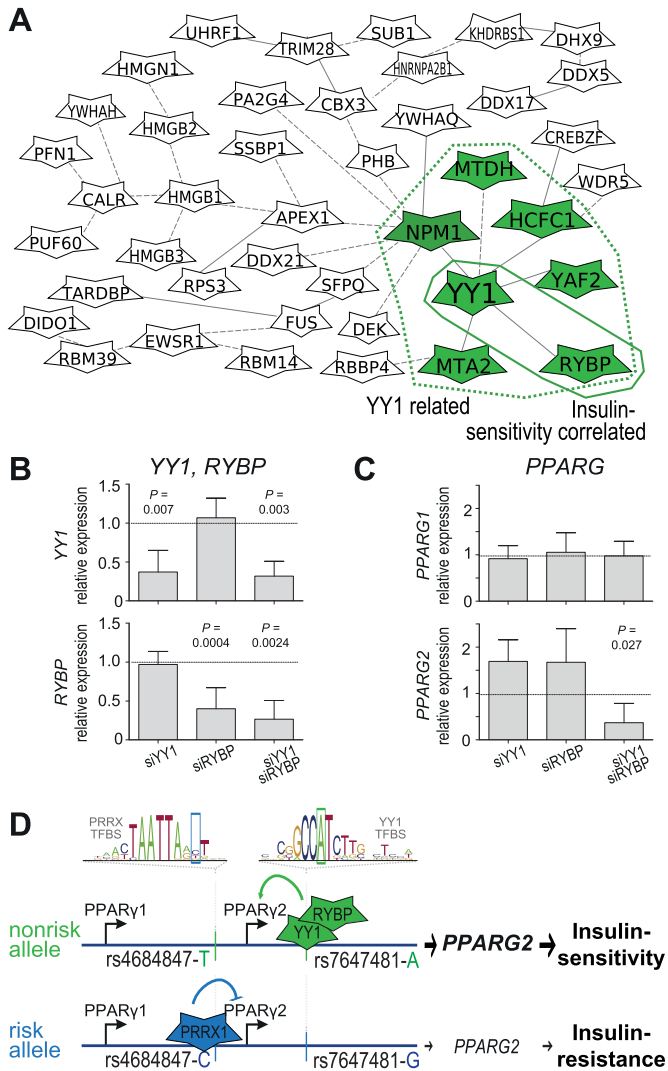
Figure 5. Interaction network analysis of YY1 with cofactors infers RYBP contribution to nonrisk allele-specific effect on insulin-resistance. (**A**) Interaction network of the YY1 transcription factor identified at the rs7647481A nonrisk allele with all transcriptional coregulators identified in the same label-free proteomics analysis. Associations by co-citation (dotted lines) or expert curation (lines) from GePS tool analysis (Genomatix, see Materials and Methods). Proteins with direct interaction to the transcription factor YY1 (green dotted line) and with positive correlation of adipose mRNA levels to insulin-sensitivity (green line) are shown (Table 2). (**B** and **C**) *YY1* and *RYBP* (**B**), *PPARG1* and *PPARG2* (**C**) mRNA expression levels measured by qPCR, standardized to *GAPDH,* in SGBS preadipocytes treated with different siRNAs for 72 h labeled as siYY1, siRYBP or siYY1+siRYBP/siNT (non-targeting control). Mean ± SD from five experiments. *P*-values from one sample *t*-test. (**D**) Impact of nonrisk and risk allele identified proteins on the *PPARG* locus phenotype insulin-resistance. The rs7647481A nonrisk allele promotes binding of YY1 and its cofactor RYBP which activate *PPARG* expression; thereby improving insulin-sensitivity. The rs4684847C risk allele binds the *PPARG* suppressor PRRX1; resulting in insulin-resistance (6).

of the allele-specific binding transcription factors *YY1, NFATC4, PRRX1* and *ILF3* (Table 1) with all identified coregulators for prioritization of in-depth proof of concept experiments. Note, that considering the second order binding of cofactors to transcription factors binding at DNA, we included all cofactors identified by proteomics

regardless of fold-change (Supplementary Table S4). In contrast to *NFATC4, PRRX1* or *ILF3,* we found a significant enrichment of reported transcriptional coregulators co-cited with *YY1* ($P = 1.56 \times 10^{-5}$, fishers exact test, Methods), i.e. RING1 and YY1 binding protein (*RYBP*), YY1 associated factor 2 (*YAF2*), prohibitin (*PHB*), nucleophosmin (*NPM1*), host cell factor C1 (*HCFC1*), metastasis associated 1 family (*MTA2*), *DEK oncogene* (*DEK*), and high mobility group box 2 (*HMGB2*). Additionally, visualizing annotated gene-gene interactions of the transcription factor *YY1* with all proteomics-identified proteins annotated as cofactors reveals a network connecting *YY1* with *RYBP, NPM1, YAF2, MTA2, HCFC1* and metadherin (*MTDH*) (Figure 5A). Co-localization of YY1 and RYBP has been reported previously by using immunofluorescence staining and co-immunoprecipitation experiments (38). *NFATC4* and *ILF3* were found connected with the cofactor calreticulin (*CALR*) and DEAH-box helicase 9 (*DHX9*), respectively, none of the identified cofactors was connected with *PRRX1* (Supplementary Figure S5A–C). For the novel cofactors which were identified by our unbiased proteomics but were not co-cited with YY1 or NFATC4 at rs7647481A nonrisk and PRRX1 or ILF3 at rs4684847C risk allele (Supplementary Table S4) further experimental proof will be necessary to support protein-protein interaction. Here, we focused on experimental proof for the YY1 / RYBP interaction.

Allele-specific correlation of transcription factor and cofactor expression levels in adipose tissue with insulin resistance

Next, we assessed if the risk and nonrisk allele-specific proteomics findings can be related to disease pathophysiology. The minor nonrisk allele of the *PPARG* locus (tagSNP rs1801282 Pro12Ala) was repeatedly associated with improved insulin-sensitivity in diverse studies. Thus, allele-specific PPARG expression may contribute to this phenotype, given the essential role of PPARG to maintain insulin-sensitivity. In fact, testing allele-specific *PPARG* mRNA levels in adipose tissue samples, we observed a confirmative age- and age/BMI-independent negative correlation of total *PPARG* mRNA levels with the insulin resistance measure HOMA-IR in nonrisk allele carriers ($\beta = -6.25$, $P = 2.18 \times 10^{-4}$; $\beta = -3.26$, $P = 0.05$, respectively) as compared to risk allele carriers ($\beta = 0.23$, $P = 0.89$; $\beta = 0.11$; $P = 0.92$, respectively, Table 2). A coordinated regulation of *PPARG* expression by YY1 and co-identified coregulators at the rs7647481A nonrisk allele may contribute to phenotypes—such as insulin-resistance—associated with the *PPARG* locus. Here, for adipose tissue mRNA expression levels of the coregulator *RYBP*, identified by proteomics and reported to interact with the YY1 transcription factor (39), we found a negative age- and age/BMI-independent correlation with HOMA-IR in individuals carrying the nonrisk ($\beta = -5.71$, $P = 1.15 \times 10^{-3}$; $\beta = -3.38$, $P = 7.04 \times 10^{-3}$; respectively) as compared to risk ($\beta = 0.57$, $P = 0.67$; $\beta = 0.16$, $P = 0.85$, respectively) allele. For none of the other proteins co-cited with YY1 or NFATC4 (Supplementary Table S5) an allele-dependent and BMI-independent correlation was observed. We found a BMI-dependent correlation of *PHB*, *CALR* and *NPM1* expres-

sion (also found at rs4684847C risk allele with PRRX1 and ILF3), requiring further analysis in the future. Taking into account the impact of BMI on insulin-sensitivity, our data support the literature-mining based initial focus on YY1 and RYBP. While we found no significant correlation of *YY1* mRNA levels with HOMA-IR in the small available data set, a confirmative direction of β-values was observed (Table 2). Finally, we also found a positive correlation for adipose mRNA expression levels of both, *YY1* and *RYBP*, with total mRNA levels of the insulin-sensitizing transcription factor *PPARG* from both alleles (Supplementary Table S5). YY1 and RYBP can function as repressor or activator depending on genomic context and availability of interaction partners (38,40). Assessing the effect on endogenous mRNA expression levels in SGBS preadipocytes, we found that knockdown of *YY1* and its cofactor *RYBP* alone (Figure 5B, 63% or 60% knockdown efficiency, $P = 7 \times 10^{-3}$ or 4×10^{-4}, respectively) resulted in a slight but not significant 1.6-fold increase of *PPARG2* expression (Figure 5C) suggesting inhibitor-activity. However, in 293T cells YY1 over-expression significantly increased rs7647481A nonrisk allele reporter activity (Figure 4C) suggesting activator-activity, possibly by recruitment of endogenously expressed RYBP (Supplementary Figure S5D). Therefore, we performed simultaneous knockdown of *YY1* and *RYBP* (Figure 5B, 68% or 73% knockdown efficiency, $P = 3 \times 10^{-3}/2 \times 10^{-3}$, respectively) in the *PPARG1* and *PPARG2* expressing adipose tissue cell line SGBS. We found a significant 2-fold reduction of endogenous mRNA expression levels for the insulin-sensitizing *PPARG2* isoform ($P = 0.027$, Figure 5C) suggesting that YY1 and RYBP jointly activate *PPARG2* expression and supporting the importance to account for both, transcription factors and related cofactors. How further cofactors identified by our unbiased proteomics approach (Supplementary Table S4) contribute to activation or inhibition of *PPARG* gene expression requires future experiments. Overall, our findings suggest that *PPARG* expression, and thereby insulin sensitivity, may be increased by rs7647481A nonrisk allele-specific binding of the transcription factor YY1 and its cofactor RYBP (Figure 5D).

DISCUSSION

GWAS revealed numerous risk loci associated with common traits (1). Advances of the ENCODE project and novel bioinformatics approaches facilitate identification of *cis*-regulatory, potentially diseases-causing variants within complex loci (2–7). However, the spatial and temporal varied expression pattern of transcription factors and coregulators supports the need to consider cell-type specific open chromatin data (2,41–45) to prioritize candidate *cis*-regulatory variants. In our study, combining computational TFBS modularity analysis (6) and functional cell type- and differentiation-specific data from human adipocytes (36) enabled identification of a second *cis*-regulatory variant at the *PPARG* locus, additional to a previously reported (6). Our unbiased quantitative label-free proteomics approach came up with significantly more allele-specific binding proteins at predicted *cis*-regulatory as compared to non *cis*-regulatory variants, supporting the integrative framework predictions. Moreover, we find both, allele-specific tran-

scription factors and cofactors which may contribute to the rs7647481A nonrisk allele-specific association of the *PPARG* locus with insulin sensitivity.

Identifying the allele-dependent binding proteins is an essential step to further decipher the molecular mechanisms underlying genetic associations with disease pathophysiology and ultimately to define personalized interventions. However, identification of allele-specific binding proteins by TFBS matrix overlap or ChIP-seq faces limitations, such as availability of TFBS matrix annotation and the complexity of TFBS modularity. So far, few proteomic studies have provided successful transcription factor identification at *cis*-regulatory variants (12,13,46). Here, taking into account the importance of TFBS modularity for specific protein–DNA interaction (6,47,48), we assessed protein binding directly at the genomic regions of interest, instead of e.g. concatenated oligonucleotides (13). Peptide intensity-based label-free quantification across samples was previously benchmarked against SILAC labeling and compared well with respect to reproducibility, sensitivity, and robustness (14). In contrast to metabolic (13,46) or chemical labeling strategies (12) our label-free approach does not limit future application to any tissue or cell type, including primary human tissue. Our proteomics workflow on eluted fractions containing allele-specific binding-proteins allows identification of allele-specific binding transcription factors. Moreover, our workflow enables for the first time the identification of transcriptional coregulators related to allele-specific gene regulation, which are among the lowest abundant proteins in cells (42,49).

The *PPARG* locus is robustly associated with type 2 diabetes and insulin-sensitivity (16–18,50,51) and mRNA levels of the insulin-sensitizing *PPARG* are increased in nonrisk allele carriers (6). At the here identified rs7647481A nonrisk allele, proteomic analysis identified allele specific binding of two transcription factors, YY1 and NFATC4. YY1 was reported to regulate metabolic, diabetes-related phenotypes in skeletal muscle, liver and adipocytes (52–56). NFATC4 contributes to regulation of *PPARG* and mouse adipocyte differentiation by direct binding at the *PPARG2* promoter (57), YY1 indirectly by interaction with C/EBPα (56). We focused on the allele-specific activity of human YY1 and found *in vivo* allele-specific binding at the rs7647481A nonrisk allele in the human *PPARG* promoter by ChIP experiments combined with assessment of allelic imbalance in heterozygous primary human adipose tissue cells, supporting the biological relevance of the proteins identified by our label-free proteomics approach. At the rs4684847C risk allele, we previously reported an overlapping homeobox TFBS, risk allele specific binding of the transcriptional inhibitor PRRX1 repressing *PPARG* expression and promoting insulin-resistance (6). Our unbiased proteomics confirmed risk allele binding of PRRX1 and also found ILF3, a transcription factor so far not related to adipose *PPARG* gene regulation or diabetes. The regulation of *PPARG* expression is complex, and future experiments are needed to support contribution of further factors, such as NFATC4 and ILF3 at rs7647481 and rs4684847, respectively, to allele-specific *PPARG* expression in human adipose tissue, but also for possible interactions of PPRX1 with ILF3 or NFATC4 with YY1.

Table 2. Risk and nonrisk allele specific correlation of adipose tissue *PPARG*, *YY1* and *RYBP* mRNA expression levels (log transformed) with the type 2 diabetes trait insulin-resistance

Gene	Allele	Adj	HOMA_IR		
			β	SE	*P*-value
PPARG	All	—	− 3.47	1.19	6.03×10^{-3}
		a	− 3.52	1.19	5.48×10^{-3}
		a.b	− 1.57	0.87	0.08
	Nonrisk	—	− 6.27	1.33	2.27×10^{-4}
		a	− 6.25	1.32	2.18×10^{-4}
		a.b	− 3.26	1.50	0.05
	Risk	—	0.25	1.68	0.88
		a	0.23	1.73	0.89
		a.b	0.11	1.10	0.92
YY1	All	—	0.07	1.59	0.96
		a	− 0.01	1.69	1.00
		a.b	− 0.25	1.08	0.82
	Nonrisk	—	− 2.87	2.63	0.29
		a	− 3.97	2.79	0.17
		a.b	− 2.33	1.70	0.19
	Risk	—	2.18	1.77	0.23
		a	2.36	1.86	0.22
		a.b	1.15	1.23	0.36
RYBP	All	—	− 1.98	1.11	0.084
		a	− 1.98	1.11	0.083
		a.b	− 1.14	0.73	0.13
	Nonrisk	—	− 5.52	1.49	1.89×10^{-3}
		a	− 5.71	1.44	1.15×10^{-3}
		a.b	− 3.38	1.09	7.04×10^{-3}
	risk	—	0.55	1.31	0.68
		a	0.57	1.31	0.67
		a.b	0.16	0.84	0.85

Gene expression was measured in adipose tissue from a lean/obese patient cohort (38 subjects. mean ± SD 24.2 ± 9.1 kg/m^2). rs7647481 and rs4684847 risk allele and nonrisk allele genotypes were determined by Sequenom-assay. *Nonrisk:* subjects heterozygous or homozygous ($n = 18$) for the rs7647481A (YY1/RYBP binding) and rs4684847T nonrisk allele; *risk:* subjects homozygous ($n = 20$) for the rs7647481G and rs4684847C risk allele. *P*-values and β-estimates from linear regression analysis of total *PPARG* mRNA levels (from microarray data measuring exons shared by both *PPARG1* and *PPARG2*), *YY1* and *RYBP* mRNA expression levels with insulin-resistance measure HOMA-IR (homeostasis model assessment of insulin resistance) are shown. Adj = correlations without adjustment (—), age (a) or age and BMI adjusted (a.b).

In addition to transcription factors, the high sensitivity of the applied proteomics approach enabled identification of several cofactors which may be involved in modulating transcriptional regulation of *PPARG*, by yet to be characterized mechanisms in future studies. For proof-of-concept that our allele-specific proteomics can find both, allele-specific transcription factors and cofactors, we selected the transcription factor YY1 with the highest allele-specific binding and the co-citation enriched RYBP cofactor at rs7647481. The coregulator RYBP—known to interact with YY1 and here co-identified at the rs7647481 variant—was recently shown to associate with skeletal myogenesis (38), in addition to its function as transcription repressor in cancer (58,59), embryogenesis (39) and central nervous system development (60). While YY1 has been reported previously to promote adipocyte differentiation (61), we found that the combined action of the transcription factor YY1 and the cofactor RYBP is necessary for full activation of *PPARG2* isoform expression in an adipocyte cell line. *PPARG2* has been reported to be crucial for maintaining insulin-sensitivity (20). In human samples we demonstrated a nonrisk allele-specific association of *RYBP* expression levels with the *PPARG* nonrisk allele associated phenotype insulin-sensitivity. Thus, in carriers of the protective *PPARG* allele, binding of YY1 and RYBP at the rs7647481A nonrisk allele may increase *PPARG2* expression and thereby insulin sensitivity (Figure 5D, upper panel); and in *PPARG* risk allele carriers the previously reported rs4684847C risk allele binding of PRRX1 inhibits

PPARG expression thereby promoting insulin-resistance (6) (Figure 5D, lower panel).

In conclusion, our results demonstrate the importance to consider allele-specific protein-complexes for delineation of the molecular mechanisms affected by *cis*-regulatory variants. We present an approach enabling an unbiased identification of allele-specific protein–DNA interactions including both, transcription factors and transcriptional cofactors. Additionally, we provide data supporting that different *cis*-regulatory variants at the *PPARG* locus may contribute to disease pathophysiology (Figure 5D), in line with the 'multiple enhancer hypothesis' suggesting multiple regulatory SNPs per LD block (62). Integrative approaches combining computational and cell type specific histone / chromatin mark based *cis*-regulatory prediction in combination with highly sensitive proteome-wide identification of allele-specific binding proteins can help to clarify the phenotypic effects of inherited and somatic genetic variability.

SUPPLEMENTARY DATA

Supplementary Data are available at NAR Online.

ACKNOWLEDGEMENTS

FUNDING

REFERENCES

1. Hindorff,L.A., Sethupathy,P., Junkins,H.A., Ramos,E.M., Mehta,J.P., Collins,F.S. and Manolio,T.A. (2009) Potential etiologic and functional implications of genome-wide association loci for human diseases and traits. *Proc. Natl. Acad. Sci. U.S.A.*, **106**, 9362–9367.

2. The ENCODE Project Consortium (2012) An integrated encyclopedia of DNA elements in the human genome. *Nature*, **489**, 57–74.

3. Schaub,M.A., Boyle,A.P., Kundaje,A., Batzoglou,S. and Snyder,M. (2012) Linking disease associations with regulatory information in the human genome. *Genome Res.*, **22**, 1748–1759.

4. Edwards,S.L., Beesley,J., French,J.D. and Dunning,A.M. (2013) Beyond GWASs: illuminating the dark road from association to function. *Am. J. Hum. Genet.*, **93**, 779–797.

5. Hoffman,M.M., Ernst,J., Wilder,S.P., Kundaje,A., Harris,R.S., Libbrecht,M., Giardine,B., Ellenbogen,P.M., Bilmes,J.A., Birney,E. *et al.* (2013) Integrative annotation of chromatin elements from ENCODE data. *Nucleic Acids Res.*, **41**, 827–841.

6. Claussnitzer,M., Dankel,S.N., Klocke,B., Grallert,H., Glunk,V., Berulava,T., Lee,H., Oskolkov,N., Fadista,J., Ehlers,K. *et al.* (2014) Leveraging cross-species transcription factor binding site patterns: from diabetes risk loci to disease mechanisms. *Cell*, **156**, 343–358.

7. Ritchie,G.R., Dunham,I., Zeggini,E. and Flicek,P. (2014) Functional annotation of noncoding sequence variants. *Nat. Methods*, **11**, 294–296.

8. Musunuru,K., Strong,A., Frank-Kamenetsky,M., Lee,N.E., Ahfeldt,T., Sachs,K.V., Li,X., Li,H., Kuperwasser,N., Ruda,V.M. *et al.* (2010) From noncoding variant to phenotype via SORT1 at the 1p13 cholesterol locus. *Nature*, **466**, 714–719.

9. Praetorius,C., Grill,C., Stacey,S.N., Metcalf,A.M., Gorkin,D.U., Robinson,K.C., Van Otterloo,E., Kim,R.S., Bergsteinsdottir,K., Ogmundsdottir,M.H. *et al.* (2013) A polymorphism in IRF4 affects human pigmentation through a tyrosinase-dependent MITF/TFAP2A pathway. *Cell*, **155**, 1022–1033.

10. Spieler,D., Kaffe,M., Knauf,F., Bessa,J., Tena,J.J., Giesert,F., Schormair,B., Tilch,E., Lee,H., Horsch,M. *et al.* (2014) Restless legs syndrome-associated intronic common variant in Meis1 alters enhancer function in the developing telencephalon. *Genome Res.*, **24**, 592–603.

11. Mouchiroud,L., Eichner,L.J., Shaw,R. and Auwerx,J. (2014) Transcriptional coregulators: fine-tuning metabolism. *Cell Metab.*, **20**, 26–40.

12. Himeda,C.L., Ranish,J.A., Angello,J.C., Maire,P., Aebersold,R. and Hauschka,S.D. (2004) Quantitative proteomic identification of six4 as the trex-binding factor in the muscle creatine kinase enhancer. *Mol. Cell. Biol.*, **24**, 2132–2143.

13. Butter,F., Davison,L., Viturawong,T., Scheibe,M., Vermeulen,M., Todd,J.A., Mann,M. and Barsh,G.S. (2012) Proteome-wide analysis of disease-associated SNPs that show allele-specific transcription factor binding. *PLoS Genet.*, **8**, e1002982.

14. Merl,J., Ueffing,M., Hauck,S.M. and von Toerne,C. (2012) Direct comparison of MS-based label-free and SILAC quantitative proteome profiling strategies in primary retinal Müller cells. *Proteomics*, **12**, 1902–1911.

15. Park,S.-S., Wu,W.W., Zhou,Y., Shen,R.-F., Martin,B. and Maudsley,S. (2012) Effective correction of experimental errors in quantitative proteomics using stable isotope labeling by amino acids in cell culture (SILAC). *J. Proteomics*, **75**, 3720–3732.

16. Deeb,S.S., Fajas,L., Nemoto,M., Pihlajamaki,J., Mykkanen,L., Kuusisto,J., Laakso,M., Fujimoto,W. and Auwerx,J. (1998) A Pro12Ala substitution in PPARγ2 associated with decreased receptor activity, lower body mass index and improved insulin sensitivity. *J. Proteomics*, **20**, 284–287.

17. Altshuler,D., Hirschhorn,J.N., Klannemark,M., Lindgren,C.M., Vohl,M.C., Nemesh,J., Lane,C.R., Schaffner,S.F., Bolk,S., Brewer,C. *et al.* (2000) The common PPAR[gamma] Pro12Ala polymorphism is associated with decreased risk of type 2 diabetes. *Nat. Genet.*, **26**, 76–80.

18. Voight,B.F., Scott,L.J., Steinthorsdottir,V., Morris,A.P., Dina,C., Welch,R.P., Zeggini,E., Huth,C., Aulchenko,Y.S., Thorleifsson,G. *et al.* (2010) Twelve type 2 diabetes susceptibility loci identified through large-scale association analysis. *Nat. Genet.*, **42**, 579–589.

19. Rosen,E.D., Sarraf,P., Troy,A.E., Bradwin,G., Moore,K., Milstone,D.S., Spiegelman,B.M. and Mortensen,R.M. (1999) PPARγ is required for the differentiation of adipose tissue in vivo and in vitro. *Mol. Cell*, **4**, 611–617.

20. Medina-Gomez,G., Virtue,S., Lelliott,C., Boiani,R., Campbell,M., Christodoulides,C., Perrin,C., Jimenez-Linan,M., Blount,M., Dixon,J. *et al.* (2005) The link between nutritional status and insulin sensitivity is dependent on the adipocyte-specific peroxisome proliferator—activated receptor-γ2 isoform. *Diabetes*, **54**, 1706–1716.

21. Tontonoz,P., Hu,E. and Spiegelman,B.M. (1994) Stimulation of adipogenesis in fibroblasts by PPARγ2, a lipid-activated transcription factor. *Cell*, **79**, 1147–1156.

22. Fajas,L., Auboeuf,D., Raspé,E., Schoonjans,K., Lefebvre,A.-M., Saladin,R., Najib,J., Laville,M., Fruchart,J.-C., Deeb,S. *et al.* (1997) The organization, promoter analysis, and expression of the human PPARγ gene, *J. Biol. Chem.*, **272**, 18779–18789.

23. Mukherjee,R., Jow,L., Croston,G.E. and Paterniti,J.R. (1997) Identification, characterization, and tissue distribution of human peroxisome proliferator-activated receptor (PPAR) isoforms PPARgamma2 versus PPARgamma1 and activation with retinoid X receptor agonists and antagonists. *J. Biol. Chem.*, **272**, 8071–8076.

24. Saladin,R., Fajas,L., Dana,S., Halvorsen,Y.D., Auwerx,J. and Briggs,M. (1999) Differential regulation of peroxisome proliferator activated receptor gamma1 (PPARgamma1) and PPARgamma2 messenger RNA expression in the early stages of adipogenesis. *Cell Growth Differ.*, **10**, 43–48.

25. Hoffmann,C., Zimmermann,A., Hinney,A., Volckmar,A.L., Jarrett,H.W., Fromme,T., Klingenspor,M. and Ko,B.C. (2013) A novel SP1/SP3 dependent intronic enhancer governing transcription of the UCP3 gene in brown adipocytes. *PLoS ONE*, **8**, e83426.

26. Schreiber,E., Matthias,P., Müller,M.M. and Schaffner,W. (1989) Rapid detection of octamer binding proteins with 'mini extracts', prepared from a small number of cells, *Nucleic Acids Res.*, **17**, 6419.

27. Kretschmer,A., Möller,G., Lee,H., Laumen,H., Toerne,C.von, Schramm,K., Prokisch,H., Eyerich,S., Wahl,S., Baurecht,H. *et al.* (2014) A common atopy-associated variant in the Th2 cytokine locus control region impacts transcriptional regulation and alters SMAD3 and SP1 binding. *Allergy*, **69**, 632–642.

28. Wisniewski,J.R., Zougman,A., Nagaraj,N. and Mann,M. (2009) Universal sample preparation method for proteome analysis. *Nat. Methods*, **6**, 359–362.

29. Hauck,S.M., Dietter,J., Kramer,R.L., Hofmaier,F., Zipplies,J.K., Amann,B., Feuchtinger,A., Deeg,C.A. and Ueffing,M. (2010) Deciphering membrane-associated molecular processes in target tissue of autoimmune uveitis by label-free quantitative mass spectrometry. *Mol. Cell. Proteomics*, **9**, 2292–2305.

30. von Toerne,C., Kahle,M., Schäfer,A., Ispiryan,R., Blindert,M., Hrabe De Angelis,M., Neschen,S., Ueffing,M. and Hauck,S.M. (2013) Apoe, Mbl2, and Psp plasma protein levels correlate with diabetic phenotype in NZO mice—an optimized rapid workflow for SRM-based quantification, *J. Proteome Res.*, **12**, 1331–1343.

31. Mueller,K., Quandt,J., Marienfeld,R.B., Weihrich,P., Fiedler,K., Claussnitzer,M., Laumen,H., Vaeth,M., Berberich-Siebelt,F., Serfling,E. *et al.* (2013) Octamer-dependent transcription in T cells is mediated by NFAT and NF-kB. *Nucleic Acids Res.*, **41**, 2138–2154.

32. Feldkotter,M., Schwarzer,V., Wirth,R., Wienker,T.F. and Wirth,B. (2002) Quantitative analyses of SMN1 and SMN2 based on real-time lightCycler PCR: fast and highly reliable carrier testing and prediction of severity of spinal muscular atrophy. *Am. J. Hum. Genet.*, **70**, 358–368.

33. Holzapfel,C., Baumert,J., Grallert,H., Müller,A.M., Thorand,B., Khuseyinova,N., Herder,C., Meisinger,C., Hauner,H., Wichmann,H.E. *et al.* (2008) Genetic variants in the USF1 gene are associated with low-density lipoprotein cholesterol levels and incident type 2 diabetes mellitus in women: results from the MONICA/KORA Augsburg case–cohort study, 1984–2002. *Eur. J. Endocrinol.*, **159**, 407–416.

34. Arner,E., Mejhert,N., Kulyte,A., Balwierz,P.J., Pachkov,M., Cormont,M., Lorente-Cebrian,S., Ehrlund,A., Laurencikiene,J., Heden,P. *et al.* (2012) Adipose tissue MicroRNAs as regulators of CCL2 production in human obesity. *Diabetes*, **61**, 1986–1993.

35. Bonora,E., Targher,G., Alberiche,M., Bonadonna,R.C., Saggiani,F., Zenere,M.B., Monauni,T. and Muggeo,M. (2000) Homeostasis model assessment closely mirrors the glucose clamp technique in the assessment of insulin sensitivity: studies in subjects with various degrees of glucose tolerance and insulin sensitivity. *Diabetes Care*, **23**, 57–63.

36. Mikkelsen,T.S., Xu,Z., Zhang,X., Wang,L., Gimble,J.M., Lander,E.S. and Rosen,E.D. (2010) Comparative epigenomic analysis of murine and human adipogenesis. *Cell*, **143**, 156–169.

37. 1000 Genomes Project Consortium. (2012) An integrated map of genetic variation from 1, 092 human genomes. *Nature*, **491**, 56–65.

38. Zhou,L., Wang,L., Lu,L., Jiang,P., Sun,H. and Wang,H. (2012) A novel target of microRNA-29, Ring1 and YY1-binding protein (Rybp), negatively regulates skeletal myogenesis. *J. Biol. Chem.*, **287**, 25255–25265.

39. Garcia,E., Marcos-Gutierrez,C., del Mar Lorente,M., Moreno,J.C. and Vidal,M. (1999) RYBP, a new repressor protein that interacts with components of the mammalian Polycomb complex, and with the transcription factor YY1. *EMBO J.*, **18**, 3404–3418.

40. Schlisio,S., Halperin,T., Vidal,M. and Nevins,J.R. (2002) Interaction of YY1 with E2Fs, mediated by RYBP, provides a mechanism for specificity of E2F function. *EMBO J.*, **21**, 5775–5786.

41. Dimas,A.S., Deutsch,S., Stranger,B.E., Montgomery,S.B., Borel,C., Attar-Cohen,H., Ingle,C., Beazley,C., Gutierrez,A.M., Sekowska,M. *et al.* (2009) Common regulatory variation impacts gene expression in a cell type-dependent manner. *Science*, **325**, 1246–1250.

42. Vaquerizas,J.M., Kummerfeld,S.K., Teichmann,S.A. and Luscombe,N.M. (2009) A census of human transcription factors. Function, expression and evolution. *Nat. Rev. Genet.*, **10**, 252–263.

43. Maurano,M.T., Humbert,R., Rynes,E., Thurman,R.E., Haugen,E., Wang,H., Reynolds,A.P., Sandstrom,R., Qu,H., Brody,J. *et al.* (2012) Systematic localization of common disease-associated variation in regulatory DNA. *Science*, **337**, 1190–1195.

44. Ward,L.D. and Kellis,M. (2012) Interpreting noncoding genetic variation in complex traits and human disease. *Nat. Biotechnol.*, **30**, 1095–1106.

45. Trynka,G., Sandor,C., Han,B., Xu,H., Stranger,B.E., Liu,X.S. and Raychaudhuri,S. (2013) Chromatin marks identify critical cell types for fine mapping complex trait variants. *Nat. Genet.*, **45**, 124–130.

46. Mittler,G., Butter,F. and Mann,M. (2008) A SILAC-based DNA protein interaction screen that identifies candidate binding proteins to functional DNA elements. *Genome Res.*, **19**, 284–293.

47. Pennacchio,L.A., Ahituv,N., Moses,A.M., Prabhakar,S., Nobrega,M.A., Shoukry,M., Minovitsky,S., Dubchak,I., Holt,A., Lewis,K.D. *et al.* (2006) In vivo enhancer analysis of human conserved non-coding sequences. *Nature*, **444**, 499–502.

48. Visel,A., Taher,L., Girgis,H., May,D., Golonzhka,O., Hoch,R.V., McKinsey,G.L., Pattabiraman,K., Silberberg,S.N., Blow,M.J. *et al.* (2013) A high-resolution enhancer atlas of the developing telencephalon. *Cell*, **152**, 895–908.

49. Simicevic,J., Schmid,A.W., Gilardoni,P.A., Zoller,B., Raghav,S.K., Krier,I., Gubelmann,C., Lisacek,F., Naef,F., Moniatte,M. *et al.* (2013) Absolute quantification of transcription factors during cellular differentiation using multiplexed targeted proteomics. *Nat. Methods*, **10**, 570–576.

50. Heikkinen,S., Argmann,C., Feige,J.N., Koutnikova,H., Champy,M.-F., Dali-Youcef,N., Schadt,E.E., Laakso,M. and Auwerx,J. (2009) The Pro12Ala PPARγ2 variant determines metabolism at the gene-environment interface. *Cell Metab.*, **9**, 88–98.

51. Dupuis,J., Langenberg,C., Prokopenko,I., Saxena,R., Soranzo,N., Jackson,A.U., Wheeler,E., Glazer,N.L., Bouatia-Naji,N., Gloyn,A.L. *et al.* (2010) New genetic loci implicated in fasting glucose homeostasis and their impact on type 2 diabetes risk. *Nat. Genet.*, **42**, 105–116.

52. He,C.Q., Ding,N.Z. and Fan,W. (2008) YY1 repressing peroxisome proliferator-activated receptor delta promoter. *Mol. Cell. Biochem.*, **308**, 247–252.

53. Blättler,S.M., Cunningham,J.T., Verdeguer,F., Chim,H., Haas,W., Liu,H., Romanino,K., Rüegg,M.A., Gygi,S.P., Shi,Y. *et al.* (2012) Yin Yang 1 deficiency in skeletal muscle protects against rapamycin-induced diabetic-like symptoms through activation of insulin/IGF signaling. *Cell Metab.*, **15**, 505–517.

54. Lu,Y., Xiong,X., Wang,X., Zhang,Z., Li,J., Shi,G., Yang,J., Zhang,H., Ning,G. and Li,X. (2013) Yin Yang 1 promotes hepatic gluconeogenesis through upregulation of glucocorticoid receptor. *Diabetes*, **62**, 1064–1073.

55. Verdeguer,F., Blättler,S.M., Cunningham,J.T., Hall,J.A., Chim,H. and Puigserver,P. (2014) Decreased genetic dosage of hepatic Yin Yang 1 causes diabetic-like symptoms. *Mol. Endocrinol.*, **28**, 308–316.

56. Han,Y., Choi,Y.H., Lee,S.H., Jin,Y.H., Cheong,H. and Lee,K.Y. (2015) Yin Yang 1 is a multi-functional regulator of adipocyte differentiation in 3T3-L1 cells. *Mol. Cell. Endocrinol.*, **413**, 217–227.

57. Yang,T.T.C., Xiong,Q., Enslen,H., Davis,R.J. and Chow,C.W. (2002) Phosphorylation of NFATc4 by p38 mitogen-activated protein kinases. *Mol. Cell. Biol.*, **22**, 3892–3904.

58. Zheng,L., Schickling,O., Peter,M.E. and Lenardo,M.J. (2001) The death effector domain-associated factor plays distinct regulatory roles in the nucleus and cytoplasm. *J. Biol. Chem.*, **276**, 31945–31952.

59. Danen-van,O.A.A., Voskamp,P., Seelen,M.C., van Miltenburg,M.H., Bolk,M.W., Tait,S.W., Boesen-de,C.J.G., Rohn,J.L., Borst,J. and Noteborn,M.H. (2004) Human death effector domain-associated factor interacts with the viral apoptosis agonist apoptin and exerts tumor-preferential cell killing. *Cell Death Differ.*, **11**, 564–573.

60. Pirity,M.K., Locker,J. and Schreiber-Agus,N. (2005) Rybp/DEDAF is required for early postimplantation and for central nervous system development. *Mol. Cell. Biol.*, **25**, 7193–7202.

61. Huang,H.Y., Li,X., Liu,M., Song,T.J., He,Q., Ma,C.G. and Tang,Q.Q. (2008) Transcription factor YY1 promotes adipogenesis via inhibiting CHOP-10 expression, *Biochem. Biophys. Res. Commun.*, **375**, 496–500.

62. Corradin,O., Saiakhova,A., Akhtar-Zaidi,B., Myeroff,L., Willis,J., Cowper-Sal lari,R., Lupien,M., Markowitz,S. and Scacheri,P.C. (2014) Combinatorial effects of multiple enhancer variants in linkage disequilibrium dictate levels of gene expression to confer susceptibility to common traits. *Genome Res.*, **24**, 1–13.